CpG Island Methylation in a Mouse Model of Lymphoma Is Driven by the Genetic Configuration of Tumor Cells

Rene Opavsky[1,2,3☯], Shu-Huei Wang[1,2,3,4☯], Prashant Trikha[1,2,3], Aparna Raval[1,2¤], Yuan Huang[1,2,3], Yue-Zhong Wu[1,2,4], Benjamin Rodriguez[1,2,3], Benjamin Keller[1,2,3], Sandya Liyanarachchi[1,2], Guo Wei[1,2,3,5], Ramana V. Davuluri[1,2], Michael Weinstein[1,2,3], Dean Felsher[6], Michael Ostrowski[1,2,3,5], Gustavo Leone[1,2,3*], Christoph Plass[1,2,4*]

1 Human Cancer Genetics Program, Department of Molecul\ar Virology, Immunology and Medical Genetics, The Ohio State University, Columbus, Ohio, United States of America, **2** Ohio State University Comprehensive Cancer Center, The Ohio State University, Columbus, Ohio, United States of America, **3** Department of Molecular Genetics, The Ohio State University, Columbus, Ohio, United States of America, **4** Department of Pathology, The Ohio State University, Columbus, Ohio, United States of America, **5** Department of Molecular and Cellular Biochemistry, The Ohio State University, Columbus, Ohio, United States of America, **6** Department of Medicine, Stanford University, Stanford, California, United States of America

Hypermethylation of CpG islands is a common epigenetic alteration associated with cancer. Global patterns of hypermethylation are tumor-type specific and nonrandom. The biological significance and the underlying mechanisms of tumor-specific aberrant promoter methylation remain unclear, but some evidence suggests that this specificity involves differential sequence susceptibilities, the targeting of DNA methylation activity to specific promoter sequences, or the selection of rare DNA methylation events during disease progression. Using restriction landmark genomic scanning on samples derived from tissue culture and in vivo models of T cell lymphomas, we found that *MYC* overexpression gave rise to a specific signature of CpG island hypermethylation. This signature reflected gene transcription profiles and was detected only in advanced stages of disease. The further inactivation of the *Pten*, *p53*, and *E2f2* tumor suppressors in *MYC*-induced lymphomas resulted in distinct and diagnostic CpG island methylation signatures. Our data suggest that tumor-specific DNA methylation in lymphomas arises as a result of the selection of rare DNA methylation events during the course of tumor development. This selection appears to be driven by the genetic configuration of tumor cells, providing experimental evidence for a causal role of DNA hypermethylation in tumor progression and an explanation for the tremendous epigenetic heterogeneity observed in the evolution of human cancers. The ability to predict genome-wide epigenetic silencing based on relatively few genetic alterations will allow for a more complete classification of tumors and understanding of tumor cell biology.

Citation: Opavsky R, Wang SH, Trikha P, Raval A, Huang Y, et al. (2007) CpG island methylation in a mouse model of lymphoma is driven by the genetic configuration of tumor cells. PLoS Genet 3(9): e167. doi:10.1371/journal.pgen.0030167

Introduction

Tumor development is driven by complex patterns of genetic and epigenetic abnormalities. A causative role for genetic alterations in cancer has been established; however, the significance of what is perhaps the most common epigenetic change associated with human and murine malignancies, alterations in DNA methylation, is less clear [1]. DNA methylation changes include loss of DNA methylation (hypomethylation) in repetitive sequences, which is an event that has been linked to chromosomal instability, and gain of DNA methylation (hypermethylation) in CpG islands, which is associated with gene repression [2,3]. Convincing evidence for the significance of CpG island or promoter hypermethylation in tumor development stems from the observation that these events are associated with silencing of tumor suppressor genes such as $p15^{INK4b}$, $p16^{INK4a}$, *BRCA1*, *VHL*, or *MLH1* [3,4]. More recent studies suggest that epigenetic mechanisms might even be involved in the expansion of premalignant cells during the early stages of tumorigenesis [5,6]. While CpG island methylation is associated with the silencing of a number of cancer-related genes, most CpG islands within the genome of the cancer cell remain unaffected [3,7]. The mechanisms involved in determining and maintaining the specificity of CpG island methylation during tumor development remain largely unknown, although several explanations for this phenomena have been provided, including differential susceptibilities of DNA sequences [8–10], the targeting of methyltransferase

Editor: Jeannie T. Lee, Massachusetts General Hospital, United States of America

Received April 6, 2007; **Accepted** August 16, 2007; **Published** September 28, 2007

A previous version of this article appeared as an Early Online Release on August 16, 2007, 2007 (doi:10.1371/journal.pgen.0030167.eor).

Abbreviations: COBRA, combined bisulfite restriction analysis; FACS, fluorescent activated cell sorting; MEF, mouse embryonic fibroblast; RLGS, restriction landmark genomic scanning; RT-PCR, reverse transcriptase PCR

To whom correspondence should be addressed. E-mail: Gustavo.Leone@osumc.edu (GL); Christoph.Plass@osumc.edu (CP)

☯ These authors contributed equally to this work.

¤ Current address: Department of Medicine, Stanford University, Stanford, California, United States of America

Author Summary

Genetic and epigenetic alterations of the genome are common features of cancers. The relationship between these two types of alterations, however, remains unclear. One type of epigenetic modification—DNA methylation in promoter sequences of genes—is of particular interest, since tumor cells have different patterns of promoter methylation than normal cells. Previous studies on human tumor samples have suggested a link between genetic alterations and the induction of aberrant DNA methylation; however, this link has been difficult to rigorously assess because of the incredible genetic heterogeneity found in human cancer. In this study, a mouse model of T cell lymphoma was used to explore the relationship between genetic and epigenetic modifications experienced by tumor cells. By introducing defined genetic changes into preneoplastic T cells of mice, such as the overexpression of the *MYC* oncogene and the ablation of tumor suppressor genes, we could carefully evaluate how these genetic changes impacted promoter methylation profiles during development of lymphomas in vivo. We found that the introduction of different genetic insults resulted in unique and diagnostic profiles of promoter methylation. Understanding how these methylation signatures contribute to tumor progression could eventually have diagnostic, prognostic, and therapeutic value for human cancers.

activity to specific promoters by oncogenes [11–13], and the selection for specific gene silencing events during tumor development [14,15].

Careful statistical analysis has led to contradicting results linking a relationship between genetic alterations and the epigenetic profile of cancer cells [16,17]. At least in colon cancer cells, defined sets of CpG island methylation events have been weakly associated with the presence of activating mutations in the *KRAS* and *BRAF* oncogenes as well as inactivating mutations in the *TP53* tumor suppressor gene [18–20]. Whether similar genetic–epigenetic relationships might exist in other cancer types is yet to be determined. The difficulty in interpreting these studies lies in the fact that, at least in part, the analysis of human tumors is confounded by tremendous genetic variability, tumor heterogeneity, and difficulties in obtaining appropriate tissue controls [21,22]. As a result, a clear causal relationship between genetic mutation, hypermethylation, and tumor development has remained speculative. Here, we have taken advantage of mouse models of T cell lymphoma to explore epigenetic alterations in normal, premalignant, and cancer cells and demonstrate that DNA methylation patterns are dependent on the genetic mutation spectrum present in a tumor cell.

Results

A CpG Island Hypermethylation Signature in a Mouse Model of T Cell Lymphoma

To study the epigenetic evolution that normal cells experience on the path to a fully malignant state, we exploited a bitransgenic mouse model in which inducible *MYC* overexpression leads to the development of T cell lymphomas [23]. In this system, the first transgene contains the human *MYC* cDNA under the control of the tetracycline-responsive minimal promoter (*Teto-MYC*) and the second transgene expresses the tetracycline activator protein under the control of the immunoglobulin heavy chain enhancer and the SRα promoter (*EμSR-tTA*; see Figure 1A). In the absence of doxycycline, tTA is expressed and mediates the transcription of the *Teto-MYC* transgene in approximately 30% of T cells. As a result, bitransgenic mice develop immature T cell lymphomas with lymph and splenic invasion and succumb to disease by 5 mo of age. Overexpression of *MYC* is a common feature of many human cancers, including Burkitt's lymphoma. The analysis of bitransgenic *EμSR-tTA;Teto-MYC* mice may thus represent a suitable mouse model to evaluate the effect of a single oncogenic event on the epigenome of a tumor cell.

We evaluated CpG island methylation in these *MYC*-induced tumors by restriction landmark genomic scanning (RLGS), a two-dimensional gel electrophoresis that measures the DNA methylation status of about 1,500–2,000 NotI methylation-sensitive restriction enzyme sites preferentially located in CpG islands [15,24]. A loss or reduction of a radiolabeled NotI DNA fragment is indicative of DNA methylation at that site, whereas an increase is indicative of either hypomethylation or amplification. Initially, we compared DNA from eight late-stage lymphomas that developed in *EμSR-tTA;Teto-MYC* mice and two control thymocyte samples derived from age-matched normal *EμSR-tTA* mice. This comparison revealed that 137 of 2,206 possible CpG islands were hypermethylated in at least one tumor, with 59 loci hypermethylated in five or more tumors and seven loci hypermethylated in all tumors (Figures 1B–1D). Statistical evaluation using a standard goodness-of-fit test indicated a nonrandom distribution of DNA methylation (p-value < 0.0001), which is similar to what has previously been reported for human malignancies [15,25–27]. The identity of 79 of the 137 hypermethylated NotI/EcoRV fragments was determined by sequencing the corresponding clones from the arrayed NotI/EcoRV genomic library as described before [21]. Of these, 65 corresponded to CpG islands located within 5′ regions of known genes (Table S1). Southern blot analysis of normal and tumor samples probed with the cloned DNA fragments confirmed tumor-specific hypermethylation in 14 of the 15 RLGS loci tested (Figures 1D and S1; Table S1). Bisulfite sequencing and combined bisulfite restriction analysis (COBRA) assays confirmed tumor-specific methylation in regions surrounding the NotI site in 29 out of the 34 CpG islands tested (Figures 1E, S1, and S2; Table S1). The discrepancy in the five CpG islands that were not confirmed by bisulfite-based methods may reflect assay-specific biases that rely on the utilization of different restriction endonuclease sites. Because hypermethylation is associated with gene silencing, we evaluated the expression of a subset of 16 genes corresponding to the hypermethylated CpG islands identified above. As determined by real-time reverse transcriptase PCR (RT-PCR) techniques, the expression of 15 from 16 randomly selected genes was significantly decreased in tumor samples relative to normal controls (Figures 1F and S1; Table S1). Together, these results identify a CpG island hypermethylation signature in a mouse *MYC*-induced lymphoma model that is associated with transcription repression and that has a similar frequency of altered methylation as previously found in human tumors [15].

Absence of Aberrant DNA Methylation in Precancerous Cells

To determine whether this tumor-specific methylation signature is established early in the neoplastic process, we examined *MYC* overexpressing cells in young mice prior to

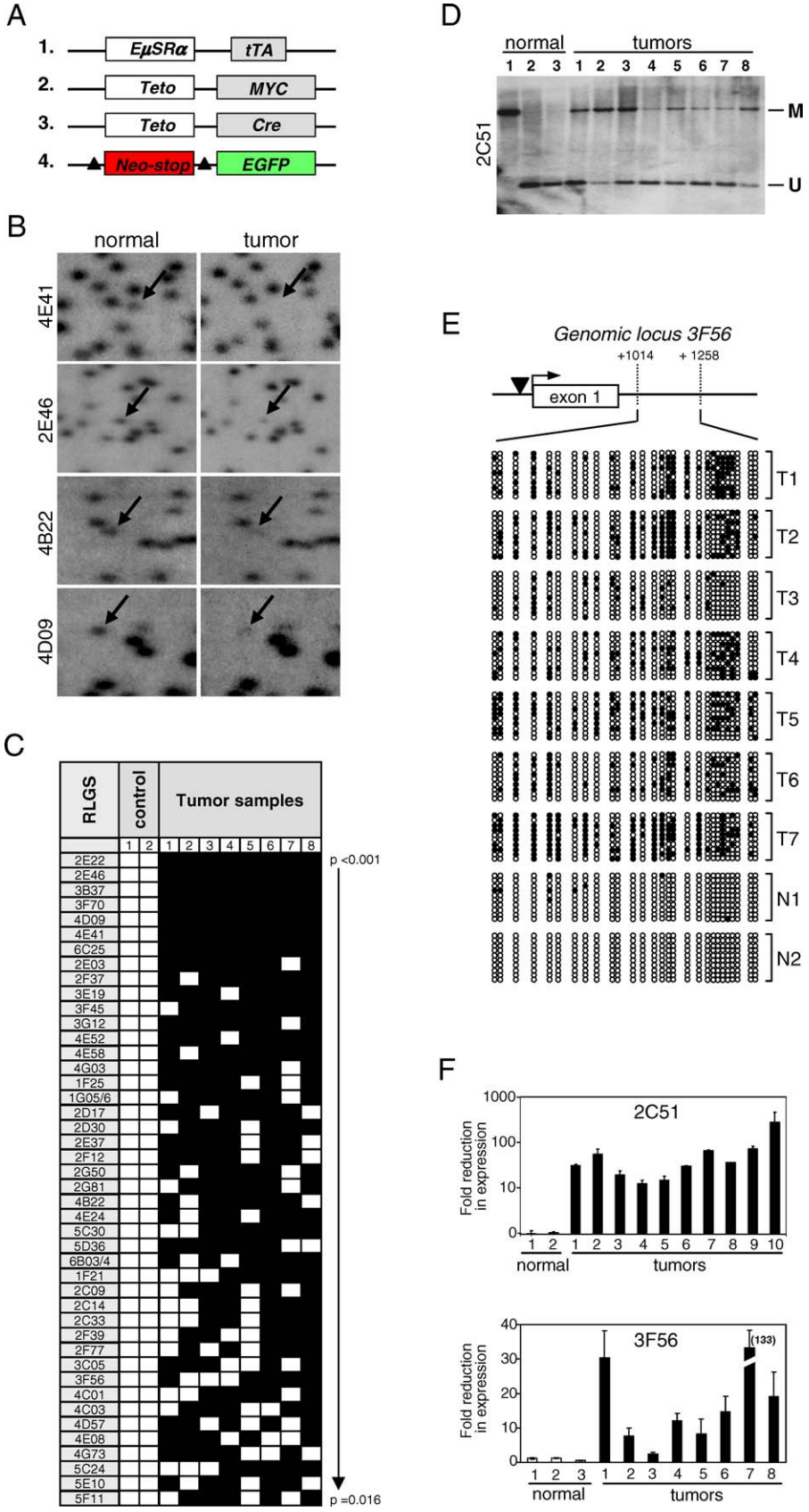

Figure 1. Signature of Aberrant DNA Methylation in *MYC*-Induced T cell Lymphomas

(A) Schematic representation of transgenes in *MYC*-induced T cell lymphoma model used in this study.

(B) Examples of RLGS profiles obtained from normal *EμSR-tTA* thymocytes (normal) and *EμSR-tTA;Teto-MYC* tumors (tumor). Loss or decreased intensity

of single-copy NotI fragments in the tumors, relative to several neighboring unaltered fragments, was detected by visual inspection of overlaid autoradiographs. The arrows indicate the position of RLGS fragments 4E41, 2E46, 4B22, and 4D09, which are lost or reduced in intensity in tumor samples, indicative of specific methylation events.
(C) Summary of the frequency of methylation events observed in eight tumor samples and two normal thymic controls. Filled boxes indicate methylation at that site and open boxes indicate no methylation. Only data for RLGS fragments that have been methylated in more than 50% of tumors are shown. Methylation data from the analysis of three sets of EGFP-positive and EGFP-negative thymocytes isolated from 21-d-old *EμSR-tTA;Teto-MYC;Teto-Cre;Rosa26LOXP*^{EGFP} mice are also shown (see text and Figure 2).
(D) Southern blot analysis of control and tumor cells using the 2C51 NotI-EcoRV DNA fragment as a probe. DNA isolated from thymocytes of *EμSR-tTA* mice was digested either with EcoRV alone (lane 1) or with EcoRV and NotI (lanes 2 and 3). DNA isolated from eight different T cell lymphomas (tumors; lanes 1–8) was digested with restriction enzymes EcoRV and NotI. The bands represent methylated (M) or unmethylated (U) NotI sites.
(E) Schematic representation of a CpG island located near the RLGS fragment 3F56. Nucleotide position of the NotI site (black triangle), exon 1, and the region amplified for bisulfite sequencing is indicated relative to the transcription initiation site. Bisulfite sequencing was performed on DNA isolated from two normal and seven tumor samples. Each circle represents a CpG dinucleotide and each row of circles indicates the sequence of an individual allele. Filled black circles correspond to methylated CpG dinucleotides and open circles represent unmethylated CpG dinucleotides.
(F) Expression of genes near the RLGS fragments 2C51 and 3F56 was quantified in thymocytes isolated from three *EμSR-tTA* mice (open bars) and eight *EμSR-tTA;Teto-MYC* tumors (black bars) using real-time RT-PCR. The *y*-axis represents fold decrease in gene expression relative to the levels of gene expression detected in the first control.
doi:10.1371/journal.pgen.0030167.g001

clonal expansion of precancerous cells and the manifestation of overt disease, as well as in mice manifesting early symptoms of disease (Figure 2A and unpublished data). At 21 and 31 d of age, bitransgenic mice are asymptomatic and the *Teto-MYC* transgene is expressed in only a portion (~30%) of total thymocytes (unpublished data). By 42 d of age, the vast majority of mice show early signs of tumor progression, such as increased thymic cellularity and changes in the expression of cell surface markers such as CD4, CD8, and CD3. To enrich for *MYC*-expressing cells and minimize contamination from normal T cells, bitransgenic mice were interbred with *Teto-Cre;Rosa26LOXP*^{EGFP} reporter mice to yield *EμSR-tTA;Teto-MYC;Teto-Cre;Rosa26LOXP*^{EGFP} quadruple transgenic offspring (Figure 1A). Cre expression from the *Teto-Cre* transgene results in the excision of the "stop cassette" located upstream of the *Rosa26LOXP*^{EGFP} locus and synthesis of EGFP. Thus, accumulation of tTA (from *EμSR-tTA*) activates the *Teto-MYC* and *Teto-Cre* transgenes and leads to the simultaneous expression of *MYC*, *Cre,* and *EGFP* within the same subpopulation of T cells. As shown in Figure 2B, fluorescent activated cell sorting (FACS)-based cell sorting of thymocytes isolated from 21-, 31- and 42-d-old quadruple transgenic mice resulted in the efficient separation of EGFP-positive and EGFP-negative thymocytes. As expected, there was a marked enrichment of *MYC* expression as well as one of its bona fide transcriptional targets, *nucleolin*, in EGFP-positive cells (Figures 2C, S4A and S4D). Surprisingly, the RLGS patterns of DNA methylation in three pairs of EGFP-positive and EGFP-negative cells derived from 21-, 31- and 42-d-old mice were identical, indicating that *MYC* overexpression in thymocytes is not sufficient to target hypermethylation to specific CpG islands (Figure 2D and 2E; unpublished data). The absence of aberrant promoter methylation at these early stages of disease was confirmed by gene-specific COBRA assays (Figures 2F and S3A–S3C).

Because promoter methylation can potentially represent a consequence of long-term repression, we measured during these early stages of lymphomagenesis the expression of genes that are typically repressed at late stages of disease. Analysis of EGFP-negative and EGFP-positive thymocytes isolated from 21-, 31- and 42-d-old *EμSR-tTA;Teto-MYC;Teto-Cre;Rosa26LOXP*^{EGFP} mice revealed no significant differences in the expression of the thirteen genes evaluated by real time PCR assays (Figures 2G, S4B, and S4E). The fact that aberrant DNA methylation and gene repression can only be detected during late stages of *MYC*-induced lymphomagenesis, once a pre-tumor cell has clonally expanded to the entire thymus and/or the periphery, suggests that rare DNA methylation events arise (or are selected for) during the course of tumor development and are not a direct consequence of *MYC* over-expression.

Overlapping CpG Island Hypermethylation Signatures Selected During In Vitro and In Vivo Transformation of Mouse Embryonic Fibroblasts

Lymphomas are thought to arise from the expansion of a small pool of cancer-initiating cells [28]. Because the cellular compartment from which tumor cells arise has not been defined in the *EμSR-tTA;Teto-MYC* model, it is impossible to ascertain the DNA methylation status of the genome in these cells. Thus, to evaluate CpG island methylation in a more homogenous and experimentally amenable cell system where the chronology of aberrant DNA methylation could be better evaluated during the early neoplastic process, we turned to mouse embryonic fibroblasts (MEFs). Primary MEFs have the potential to be transformed in vitro and in vivo by the cointroduction of two oncogenes. We thus compared DNA methylation by RLGS methods in primary MEFs before and immediately after their transformation with *MYC* and an activated form of *Ras* (*Ras*^{61L}). This comparison of 1,635 NotI restriction sites revealed no methylation changes between control and fully transformed *MYC/Ras*^{61L}-expressing cells (Figure 3A–3C), suggesting that as in *EμSR-tTA;Teto-MYC* mice, *MYC* expression and transformation of MEFs is not sufficient to target methylation to specific CpG islands. We then assessed whether signatures of CpG island methylation could be acquired or selected for when transformed MEFs are cultured for longer periods of time. DNA methylation was analyzed in *MYC/Ras*^{61L}-transformed MEFs that were either cultured in vitro for several weeks or were injected into nude mice for an equivalent length of time (Figure 3A). Approximately 17 NotI sites were found to be hypermethylated in *MYC/Ras*^{61L}-transformed MEFs cultured in vitro and an additional seven NotI sites were hypermethylated in tumor cells that emerged in the injected nude mice (Figure 3B and 3C). These data suggest that among all *Myc/Ras*^{61L}-expressing MEFs with a fully transformed phenotype, only those with a specific pattern of methylated CpG islands are favored during their in vitro or in vivo expansion. The additional DNA methylation events observed in tumors in nude mice presumably reflect the additional level of selection pressure

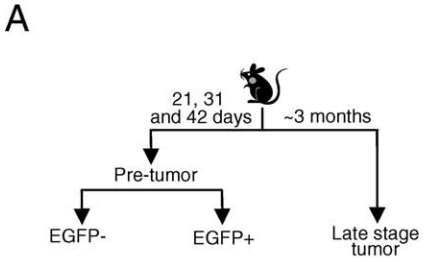

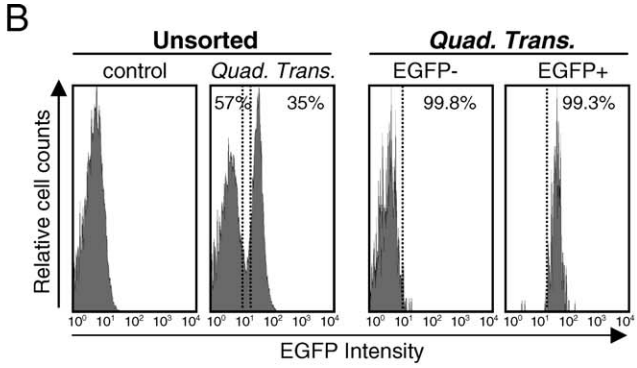

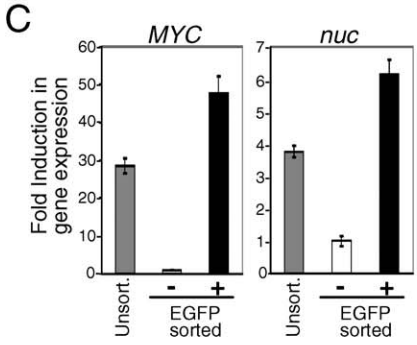

E

RLGS fragm.	% Meth.	EGFP-			EGFP+		
		1	2	3	1	2	3
2E46	100.0						
3B37	100.0						
3F70	100.0						
4E41	100.0						
6C25	100.0						
2E03	87.5						
2F37	87.5						
3F45	87.5						
3G12	87.5						
4E52	87.5						
4E58	87.5						
4G03	87.5						
2D17	75.0						
2D30	75.0						
2F12	75.0						
2G50	75.0						
2G81	75.0						
4B22	75.0						
4E24	75.0						
5C30	75.0						
5D36	75.0						
6B03/4	75.0						
1F21	62.5						
2C14	62.5						
2C33	62.5						
2F39	62.5						
2F77	62.5						
3F56	62.5						
4C01	62.5						
4C03	62.5						
4D57	62.5						
4G73	62.5						
5E10	62.5						
5F11	62.5						

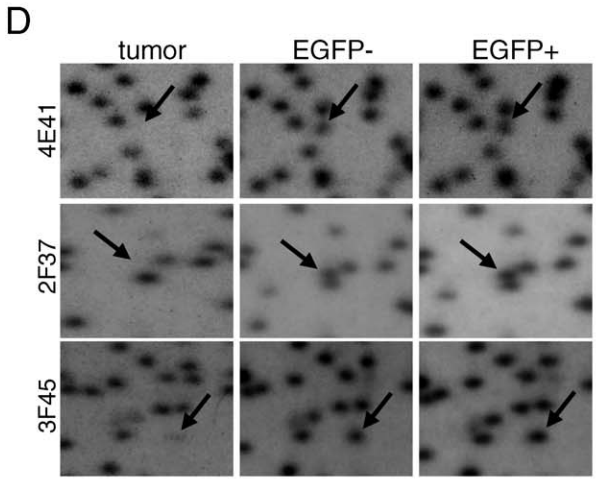

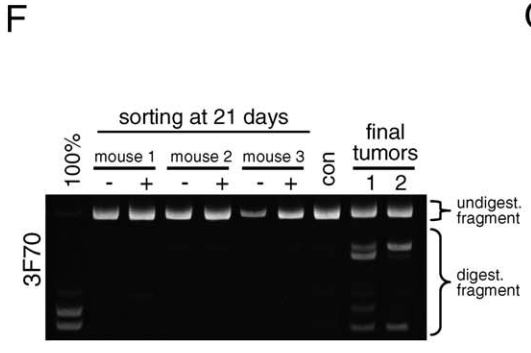

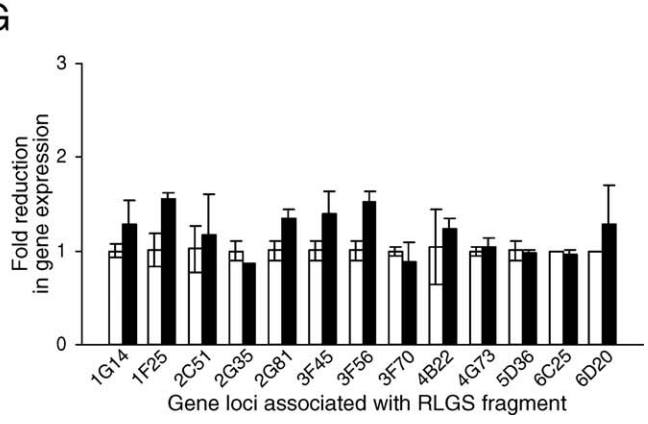

Figure 2. DNA Methylation Is Absent Early During Tumor Development

(A) Schematic representation of experimental design used in this study.

(B) *EμSR-tTA;Teto-MYC;Teto-Cre;Rosa26LOXP*^{EGFP} mice were harvested at 21 d of age, and EGFP-positive and EGFP-negative thymocytes were isolated using high-speed FACS. Flow diagrams for nontransgenic controls (EGFP-control), as well as for *EμSR-tTA;Teto-MYC;Teto-Cre;Rosa26LOXP*^{EGFP} thymocytes

prior to sorting (unsorted), and after sorting (EGFP-negative [–] and EGFP-positive [+] cells) are shown. The purity of EGFP-negative and EGFP-positive populations sorted from either side of the threshold, which is indicated with dotted lines, is shown within each panel.
(C) Real-time RT-PCR analysis of *MYC* and *nucleolin* (*nuc*) expression in unsorted (gray bars), EGFP-positive (black bars) and EGFP-negative (white bars) cell populations sorted from thymocytes of *EμSR-tTA;Teto-MYC;Teto-Cre;Rosa26LOXP*^{EGFP} mouse as described in Figure 2B. Expression data are presented as fold increase relative to the EGFP-negative population. Representative example from three independent experiments is shown.
(D) Representative examples of RLGS profile sections derived from cells isolated as described in Figure 2B. The arrows indicate the position of RLGS fragments that appear methylated in tumors.
(E) No differences in CpG methylation profiles between EGFP+ and EGFP− cell populations were detected for any of the three pairs of samples analyzed as summarized in Figure 2E where open boxes indicate no methylation at that site. Frequency of methylation events in final tumors for each RLGS fragment is shown as a percentage in corresponding boxes.
(F) COBRA analysis of bisulfite-treated DNA isolated from EGFP-negative [–] and EGFP-positive [+] thymocytes of three quadruple transgenic mice at age 21 d. PCR products for RLGS fragment 3F70 were digested with restriction enzyme BstUI and loaded onto a PAGE gel along with 100% methylated (SssI-treated DNA) control (100%). DNA from normal thymocytes (con) and two tumors is also shown. Undigested and digested fragments correspond to unmethylated and methylated DNA, respectively.
(G) Expression of genes near the RLGS fragments as determined by real-time RT-PCR analysis of EGFP-negative (white bars) and EGFP-positive (black bars) cell populations sorted from thymocytes of *EμSR-tTA;Teto-MYC;Teto-Cre;Rosa26LOXP*^{EGFP}. Expression of each gene in EGFP-positive population is presented as fold decrease relative to the expression of the same gene in EGFP-negative population. Representative examples from three independent experiments are shown.
doi:10.1371/journal.pgen.0030167.g002

that *MYC/Ras*^{61L}-transformed cells were exposed to in the in vivo setting.

Tumor Suppressor Function Drives the Specificity of CpG Island Methylation

Aberrant DNA methylation in T cell tumors could result from rare random events selected for in neoplastic cells, from specific defects in the DNA methylation process, from intrinsic sequences predisposing to DNA methylation, or a combination of all three. Genes that are methylated and silenced in cancer are likely to be involved in specific pathways impacting any number of important processes, including proliferation, differentiation, and apoptosis. We reasoned that if DNA methylation events are selected for in neoplastic cells, and therefore contribute to the neoplastic process, the inactivation of key tumor suppressors impacting one or more of these same processes might diminish the selective pressure imposed during neoplastic progression. The inactivation of tumor suppressor function would thus be predicted to change the specific DNA methylation signature acquired by tumor cells.

To test this prediction, we evaluated CpG island methylation in T cell lymphomas that developed in *EμSR-tTA;Teto-MYC* animals deleted for the *p53*, *Pten,* or *E2f2* tumor suppressors. *P53* and *PTEN* are the most frequently inactivated tumor suppressor genes in human cancer [29,30] and have been shown to have tumor suppressor function in T cells [31,32]. Recent studies in our laboratory indicate that *E2f2* expression is significantly decreased in a number of human hematopoietic malignancies and its loss in mice accelerates T cell lymphomagenesis (G. L., unpublished data). Therefore, we interbred *EμSR-tTA;Teto-MYC* and *p53*$^{-/-}$ or *E2f2*$^{-/-}$ mice to generate cohorts of *EμSR-tTA;Teto-MYC;p53*$^{-/-}$ and *EμSR-tTA;Teto-MYC;E2f2*$^{-/-}$ animals. Because germ line inactivation of *Pten* results in embryonic lethality, *EμSR-tTA;Teto-MYC* mice were interbred with mice carrying the *Teto-Cre* transgene and a conditional allele of *Pten* (*Teto-Cre;Pten*^{LoxP}). From these latter crosses we generated cohorts of *EμSR-tTA;Teto-MYC;Teto-Cre;Pten*$^{LoxP/LoxP}$ mice. Consistent with their tumor suppressor functions, loss of *p53*, *Pten*, or *E2f2* significantly accelerated disease progression ($p = 0.001$; $p = 0.005$, and $p = 0.0007$, respectively; Figure 4A). In each case, FACS analysis confirmed that lymphomas in these mice were of T cell origin and consisted of either CD4 single- or CD4/CD8 double-positive cells (Figure 4B). We then analyzed the pattern of CpG island methylation in each tumor cohort by RLGS (Figures 4C and 5A). All four tumor groups had significant amounts of promoter hypermethylation; with an average of 1.8% of CpG islands hypermethylated in the *EμSR-tTA; Teto-MYC* cohort, 1.1 % in *EμSR-tTA; Teto-MYC; p53*$^{-/-}$ cohort ($p = 0.06$), 0.3% in *EμSR-tTA; Teto-MYC; Teto-Cre;Pten*$^{LoxP/LoxP}$ ($p = 0.004$), and 1.9% in *EμSR-tTA; Teto-MYC; E2f2*$^{-/-}$ ($p = 0.885$). Importantly, there was no detectable aberrant DNA methylation in control thymocytes isolated from age-matched *EμSR-tTA;p53*$^{-/-}$, *EμSR-tTA;Teto-Cre;Pten*$^{LoxP/LoxP}$, or *EμSR-tTA;E2f2*$^{-/-}$ mice (unpublished data). The aberrant DNA methylation detected in tumor samples was confirmed by 126 COBRA reactions performed on the same tumor samples that were used for RLGS analysis. This analysis revealed that in 74% of the cases evaluated, RLGS and COBRA assays yielded identical results (Figure S5 and unpublished data). In 22 % of cases COBRA detected aberrant DNA methylation events that were not identified by RLGS. This is not surprising, since COBRA is a more sensitive method to detect DNA methylation. In 4% of cases, COBRA assays failed to detect DNA methylation events that were detected by RLGS; this discrepancy likely reflects the different restriction sites analyzed by these methods.

Side-by-side comparison of DNA methylation profiles between deleted and nondeleted tumor groups could distinguish three classes of DNA methylation events (Figure 5A). The first class included aberrant DNA methylation events that were common between deleted and nondeleted tumor cohorts, with methylation of some CpG islands occurring in all tumor groups irrespective of the particular tumor suppressor deleted. The second class consisted of aberrant DNA methylation events that were suppressed by loss of tumor suppressor function, with some DNA methylation events suppressed only in specific tumor suppressor cohorts and others events suppressed in all tumor suppressor cohorts. Conversely, the third class consisted of novel DNA methylation events that occurred in tumors as a result of tumor suppressor inactivation (Class I, Class II, and Class III; Figure 5A). An evaluation of gene expression in each tumor suppressor cohort indicated that suppression of promoter methylation correlates well with their reactivation of expression. For example, expression of *6D20*, which was methylated and silenced in 50% of *MYC*-initiated tumors, was preferentially reactivated in tumors deficient either for *E2f2, p53*, or *PTEN* (Figure 4D). Similarly, expression of seven

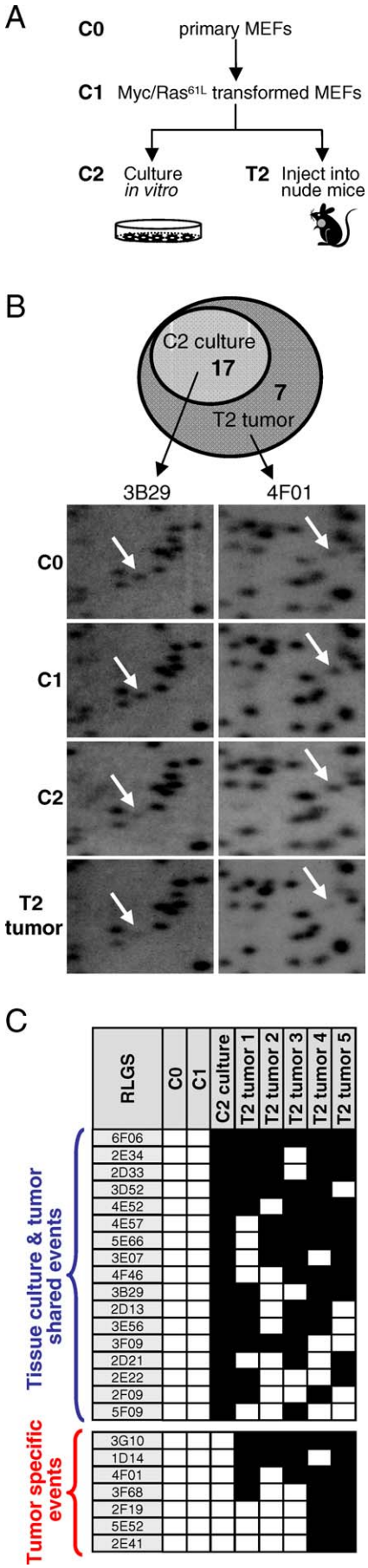

Figure 3. Aberrant DNA Methylation in Mouse Embryonic Fibroblasts Transformed with *Myc* and *Ras*

(A) Schematic representation of experimental design used for evaluation of in vitro and in vivo DNA methylation in MEFs. Early passage of primary MEFs was either harvested (C0) or infected with retroviral vectors expressing *MYC* and an activated form of *Ras* (Ras^{61L}). A portion of cells was harvested immediately after transformation had occurred, as determined by morphological changes (C1). At this point, the rest of the cells was either injected subcutaneously into nude mice or kept in culture. By 18 d, injected cells formed tumors that were harvested along with C1 cells kept in culture in vitro (T2 tumor and C2 culture, respectively).

(B) Methylation status of 1,635 NotI restriction sites was evaluated by RLGS in DNA from C0, C1, and C2 cultures along with five T2 tumors derived from nude mice. The Venn diagram shows the number of NotI fragments that became methylated in T2 culture and T2 tumors. Sections of RLGS profiles are shown for fragments 3B29 and 4F01.

(C) Summary of DNA methylation changes observed in C0, C1, and C2 culture and five T2 tumors as determined by RLGS. Open squares represent unmethylated sequences, black squares represent methylated events.

doi:10.1371/journal.pgen.0030167.g003

additional genes corresponding to RLGS fragments 2G81, 3F45, 3F56, 4B22, 1G05–06, 1D14, and 6C25 correlated well with the methylation status of CpG islands in each corresponding genetic group (Figure 4E). Additional genetic changes in the evolving tumors likely account for the few cases where expression and DNA methylation profiles did not correspond (see 1D14, $p53^{-/-}$ for an example). These data suggest that tumor suppressor–specific patterns of CpG island methylation correspond with global gene expression profiles.

As a measure of CpG methylation specificity provoked by the inactivation of individual tumor suppressor pathways, we performed a two-dimensional unsupervised hierarchical cluster analysis. This unbiased analysis of DNA methylation identified deleted ($p53^{-/-}$, $Pten^{-/-}$, and $E2f2^{-/-}$) and nondeleted tumor groups correctly (Figure S6). Strikingly, unsupervised hierarchical clustering performed with all tumor samples together led to an almost perfect segregation of tumors based on their genetic background (Figure 5B). While the entire constellation of methylation changes (or lack thereof) can serve to discriminate between genetic groups, it is clear from the data shown in Figure 5A that different methylation events contribute to different degrees. The contribution of each DNA methylation event to the clustering observed in Figure 5B was evaluated by a Random Forrest analysis and statistical ranking (see Table S4). Two important conclusions can be drawn from these experiments. The first and perhaps most obvious of these is that loss of tumor suppressor functions yield specific profiles of CpG island methylation in cancer. We view these results to mean that different tumor suppressor pathways impose unique selective pressures on neoplastic cells that drive the specificity of CpG island methylation. Interestingly, the overall frequency of hypermethylated CpG islands in *Pten*-deficient tumors was substantially less than seen in the other tumor cohorts (0.3%, $p = 0.004$), suggesting a particularly strong diversion of the selective pressure in the evolution of $Pten^{-/-}$ tumors. This suppression of tumor-specific DNA methylation by loss of *Pten* is likely a reflection of the broader number of pathways that Pten action impacts to prevent tumorigenesis [33]. The second conclusion is that the specificity of CpG island methylation is not likely to be a consequence of a general

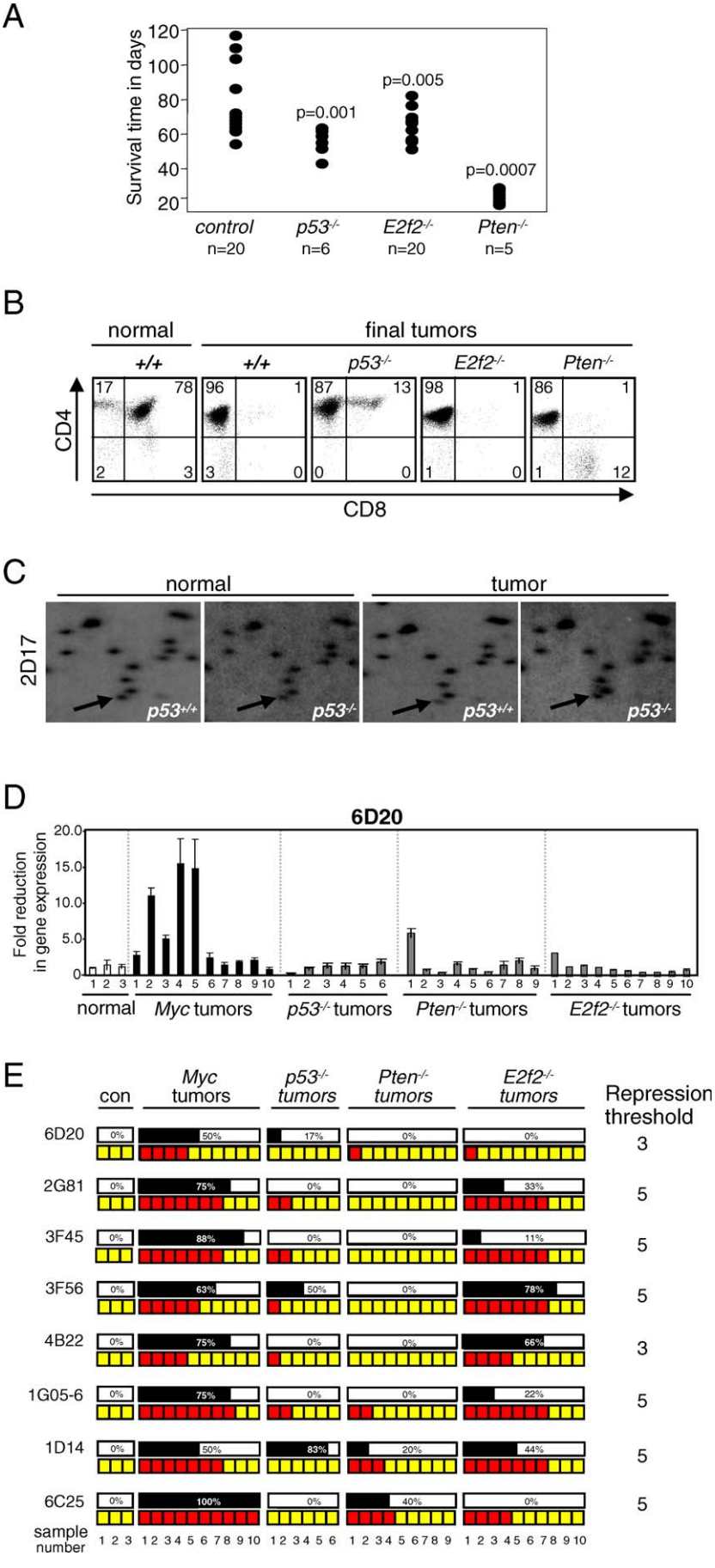
A
Survival time in days
120
100
80
60
40
20
p=0.001
p=0.005
p=0.0007
control
n=20
p53-/-
n=6
E2f2-/-
n=20
Pten-/-
n=5
B
normal
final tumors
+/+
+/+
p53-/-
E2f2-/-
Pten-/-
CD4
CD8
17
78
2
3
96
1
3
0
87
13
0
0
98
1
1
0
86
1
1
12
C
normal
tumor
2D17
p53+/+
p53-/-
p53+/+
p53-/-
D
6D20
Fold reduction in gene expression
20.0
15.0
10.0
5.0
0
normal
Myc tumors
p53-/- tumors
Pten-/- tumors
E2f2-/- tumors
E
con
Myc tumors
p53-/- tumors
Pten-/- tumors
E2f2-/- tumors
Repression threshold
6D20
0%
50%
17%
0%
0%
3
2G81
0%
75%
0%
0%
33%
5
3F45
0%
88%
0%
0%
11%
5
3F56
0%
63%
50%
0%
78%
5
4B22
0%
75%
0%
0%
66%
3
1G05-6
0%
75%
0%
0%
22%
5
1D14
0%
50%
83%
20%
44%
5
6C25
0%
100%
0%
40%
0%
5
sample number
1 2 3 1 2 3 4 5 6 7 8 9 10 1 2 3 4 5 6 1 2 3 4 5 6 7 8 9 1 2 3 4 5 6 7 8 9 10

Figure 4. Analysis of Aberrant DNA Methylation in *p53*–, *E2f2*–, and *Pten*-Deleted Lymphomas

(A) Graphical representation of the time-frame of tumor onset in *EμSR-tTA;Teto-MYC* (wild type), *EμSR-tTA;Teto-MYC;p53*$^{-/-}$ (*p53*$^{-/-}$), *EμSR-tTA;Teto-MYC;E2f2*$^{-/-}$ (*E2f2*$^{-/-}$), or *EμSR-tTA;Teto-MYC;Teto-Cre;Pten*$^{LoxP/LoxP}$ (*Pten*$^{-/-}$) mice.

(B) Examples of FACS profiles of normal thymocytes (normal) and tumor cells (tumors) derived from the different genetic backgrounds as indicated. The percentage of cells that are in each quadrant of the FACS profile is indicated.

(C) Representative examples of RLGS profile sections of normal thymocytes derived from *EμSR-tTA* (normal *p53*$^{+/+}$) and *EμSR-tTA*; *p53*$^{-/-}$ (normal *p53*$^{-/-}$) mice and tumors derived from *EμSR-tTA;Teto-MYC* (tumor *p53*$^{+/+}$) and *EμSR-tTA;Teto-MYC; p53*$^{-/-}$ (tumor *p53*$^{-/-}$) mice. The position of DNA fragment 2D17 is indicated with arrows. Note the increase in the intensity of 2D17 in tumors deleted for the *p53* tumor suppressor (compare *p53*$^{+/+}$ and *p53*$^{-/-}$ tumor samples in the third and fourth panels).

(D) Real time RT-PCR analysis of expression of 6D20 in normal thymic controls (white bars), *EμSR-tTA;Teto-MYC* tumors (black bars), or *EμSR-tTA;Teto-MYC* tumors deleted either for *p53*, *E2f2*, or *Pten* (grey bars) as indicated.

(E) Summary of expression data from tumors derived in different genetic backgrounds obtained on analysis of eight RLGS fragments as indicated. Red boxes represent tumors with reduction in expression relative to normal thymic controls; yellow boxes indicate tumors with no change in expression. Repression thresholds for individual genes were chosen as described in Materials and Methods.

doi:10.1371/journal.pgen.0030167.g004

defect in the DNA methylation machinery since the specific profile, but not the frequency, of tumor-dependent CpG methylation events is altered by the loss of *p53* or *E2f2*.

Discussion

In this study, we have investigated the interplay between genetic mutations and the establishment of global DNA methylation patterns in the development of mouse T cell lymphomas. The model used here, developed by Felsher and colleagues, uses high levels of MYC expression to mimic similar events taking place during human lymphomagenesis such as in Burkitt's lymphoma ([34] and references therein). The clear advantage of using a mouse model to study the role of DNA methylation in cancer is that cohorts used are genetically homogeneous in all respects except on a defined set of genetic variables (i.e., overexpression of MYC). Therefore, we consider this mouse model to be suitable for studying the relationship between genetic and epigenetic changes during tumor development. We demonstrate that DNA methylation patterns in these tumors are characterized by frequent and nonrandom patterns, similar to what has been described in human malignancies. These patterns are exquisitely dependent on the genetic makeup of the tumor cell, as homozygous deletion of either *p53*, *Pten*, or *E2f2* in *MYC*-induced T cell lymphomas resulted in unique tumor-specific patterns of genome-wide DNA methylation. This analysis provides the first clear-cut experimental evidence showing that genetic background can drive the establishment of aberrant DNA methylation profiles during lymphoma development, offering an explanation for the tremendous epigenetic heterogeneity observed in human cancer [4,15].

Multiple mechanisms have been proposed to explain the specificity of aberrant DNA methylation in human cancer, including the differential susceptibility of DNA sequences to methylation [8–10] and the targeting of methyltransferase activity to specific promoter sequences [12,13]. The fact that our RLGS analysis identified a specific signature of CpG island methylation that could only be detected late in the *MYC*-induced neoplastic process suggests that MYC overexpression is insufficient to target the DNA methylation machinery to specific sites. It is unlikely that the absence of aberrant promoter methylation early in the neoplastic process was due to the notoriously slow nature of de novo methylation relative to the kinetics of gene repression, since repression was not observed at these early stages of disease, either. This view is further supported by the absence of any hypermethylation signature in cells immediately following the transformation by *MYC* and *Ras*^{61L}. Rather, specific patterns of DNA methylation could only be detected in *MYC/Ras*^{61L}-transformed MEFs that have been either cultured in vitro for an extended period of time or injected into nude mice for an equally long time. However, we cannot rule out that MYC-initiated targeting of the DNA methylation machinery could occur as an infrequent aberrant event during tumor development. Comparison of global methylation profiles between different mouse models of T cell lymphomas would not only help to answer this question but it would also address to what degree the global DNA methylation pattern is dependent on initial oncogenic insult.

The work described here provides an alternative explanation for the longstanding question of tumor-specific CpG island hypermethylation. We find that tumor-specific signatures of CpG island methylation can only be detected late in the neoplastic process, at a time when the clonal expansion of pretumor cells can be observed, suggesting that specific profiles of CpG island methylation arise from the expansion of rare neoplastic cells. While we cannot rule out the possibility that DNA methylation profiles of late-stage tumor cells may indirectly reflect the selection of cells having a unique expression profile, our observation that inactivation of different tumor suppressor pathways results in distinct aberrant DNA methylation signatures indicates that rare DNA methylation events are selected for during the course of tumor development.

The function of genes silenced by hypermethylation is expected to provide tumor cells with some selective advantage. Indeed, many of the hypermethylated genes identified by RLGS have functions consistent with a tumor suppressor role, including *Id4* and *Ptprk* [22,35]. The observation that inactivation of different tumor suppressor pathways results in distinct aberrant DNA methylation signatures further supports the notion that rare DNA methylation events are selected for during the course of tumor development. We envision that the function of genes that are no longer selected for hypermethylation in each of the three tumor suppressor cohorts studied here must be somehow related or dependent on the function of the specific tumor suppressor targeted for inactivation. The inactivation of *Pten*, for example, would thus diminish the selective pressure imposed during neoplastic progression for genes involved in similar or related functions. Comparison among the three tumor suppressor cohorts suggested that this selection is strongly influenced by the specific tumor suppressor inactivated in the tumor cell. Remarkably, the strength of the influence that genetics has on this selection mechanism is illustrated by the ability of

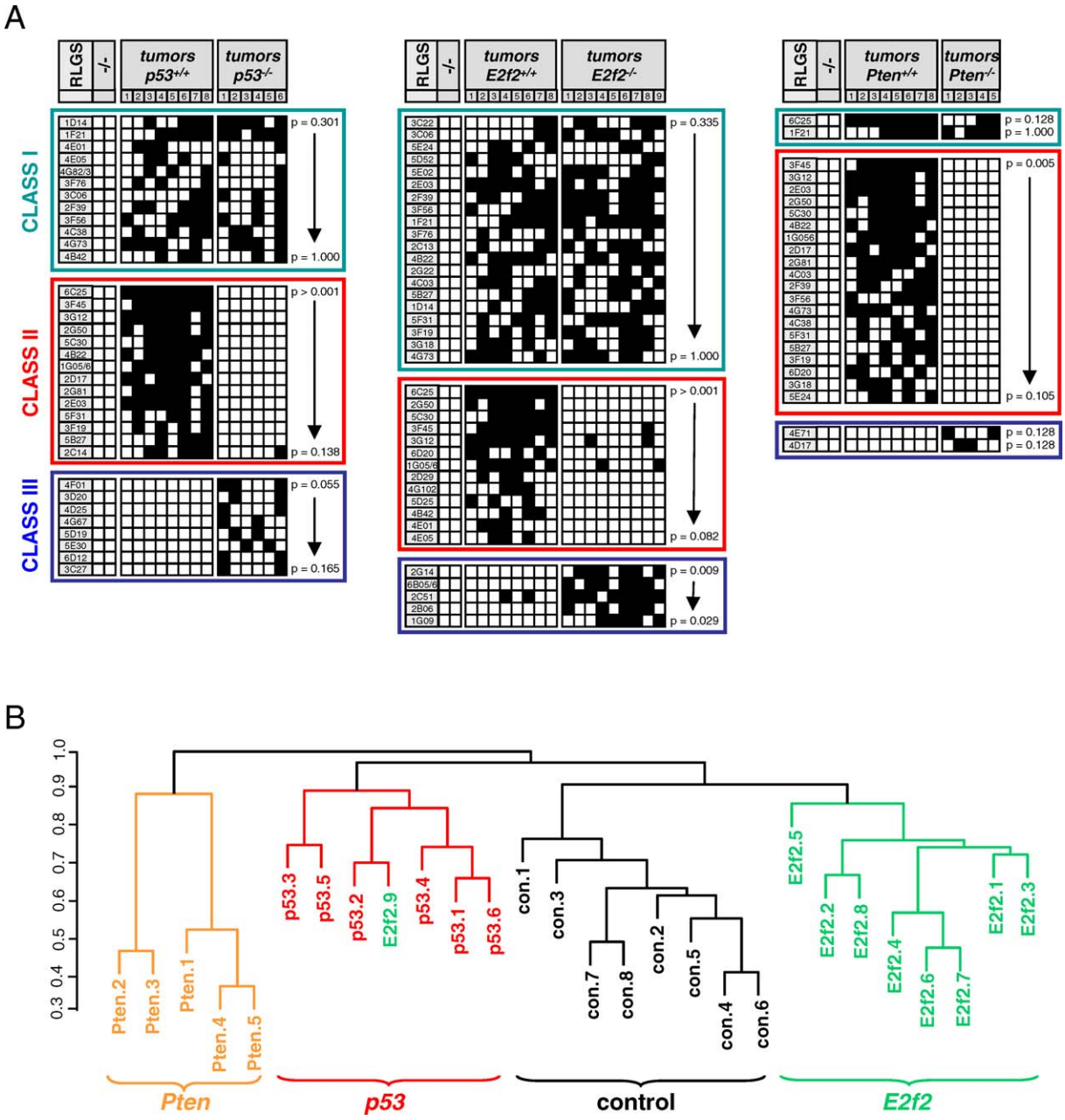

Figure 5. Loss of Tumor Suppressor Genes Redirects the Course of Aberrant DNA Methylation

(A) Comparison of tumor-specific DNA methylation changes observed in EμSR-tTA;Teto-MYC;$p53^{-/-}$ (*left panel*), EμSR-tTA;Teto-MYC;$E2f2^{-/-}$ (middle panel), and EμSR-tTA;Teto-MYC; Teto-Cre;$Pten^{LoxP/LoxP}$ (right panel) mice relative to EμSR-tTA;Teto-MYC mice (indicated as $p53^{+/+}$, $E2f2^{+/+}$, and $Pten^{+/+}$ in each of the panels). Data is shown for RLGS fragments methylated in >33% of tumors. Filled boxes indicate methylation and open boxes indicate a loss of methylation at those sites. Class I, Class II, and Class III RLGS DNA fragments are outlined in green, red, and blue, respectively). Data from analysis of thymocytes isolated from two age-matched normal control EμSR-tTA;$p53^{-/-}$ (–/–; left panel), EμSR-tTA;$E2f2^{-/-}$ (–/–; middle panel), and EμSR-tTA;Teto-Cre;$Pten^{LoxP/LoxP}$ (–/–; right panel) mice are also shown. Fisher's exact test was applied and *p*-values are shown.

(B) Dendrogram of a two-dimensional unsupervised hierarchical cluster analysis for 28 tumors analyzed using methylation status of 1,481 NotI fragments. Control (EμSR-tTA;Teto-MYC), *p53* (EμSR-tTA;Teto-MYC; $p53^{-/-}$), *E2f2* (EμSR-tTA;Teto-MYC; $E2f2^{-/-}$), or *Pten* (EμSR-tTA;Teto-MYC; Teto-Cre;$PTEN^{LoxP/LoxP}$).

doi:10.1371/journal.pgen.0030167.g005

unbiased statistical algorithms to faithfully predict the tumor suppressor status in each tumor. We would predict that the nature of the initiating oncogenic insult, in this case MYC, would have an equally important role in determining the CpG methylation profile of the emerging tumor.

It is clear from in vitro experiments and more recent genome-wide sequencing efforts that the transformation of both human and mouse cells to a malignant phenotype requires multiple sequential genetic lesions. In the context of an evolving tumor, it is likely that the initial genetic insult acts as a driving force for the first round of epigenetic alterations and that subsequent genetic alterations as the tumor evolves lead to further epigenetic selection. There is also evidence that epigenetic alterations influence the

evolution of genetic lesions. For example, it has been shown, that the hypermethylation and silencing of the mismatch repair gene *MLH1* leads to microsatellite instability in colon cancer [36,37]. Similarly, the silencing induced by promoter hypermethylation of the Werner syndrome gene that occurs in several human cancer types, leads to chromosomal instability and apoptosis [38]. Thus, the coevolution of genetic and epigenetic changes during the transformation of a normal cell may be viewed to fuel the diversity of tumor phenotypes. This interpretation is consistent with the heterogeneity of DNA methylation we observe even within a single genetic cohort of mouse lymphomas.

While the underlying mechanisms for this selection process are unknown, one could speculate that due to the loss of tumor suppressor function, gene-expression profiles are changed. These changes in gene expression may trigger a cascade of epigenetic events including nucleosome repositioning, histone tail modifications, and subsequently DNA methylation [39–41]. There is indeed evidence that a similar mechanism for the specificity of CpG island methylation is also operative in human malignancies. For example, Weisenberger et al. described the tight association of *BRAF* mutation with a CpG island methylator phenotype in colon cancer [19], and it is known that in breast cancers with either *BRCA1* or *BRCA2* mutations stable epigenetic changes reflect gene-expression profiles in these cells [42–44]. In conclusion, our findings suggest that genetic events can determine the course in the epigenetic evolution of DNA methylation during tumor development.

Materials and Methods

Generation and maintenance of mice. The *E2f2*$^{-/-}$, *Teto-Cre*, and *EμSR-tTA;Teto-MYC* mice were obtained from Stuart Orkin (Harvard Medical School, Boston, Massachussetts), Andreas Nagy (Samuel Lunenfeld Research Institute, Toronto, Canada) and Dean W. Felsher (Stanford University, Stanford, California), respectively. Mice carrying the conditional *Pten* allele (*Pten*^{LoxP}) were a generous gift from Michael Weinstein (The Ohio State University, Columbus, Ohio). Mice carrying *Rosa26LOXP*^{EGFP} allele (C57BL/6J background) were purchased from The Jackson Laboratory. Genomic DNA isolated from mouse tails was used in PCR-based genotyping. For this study, standard genetic crosses were used to generate *EμSR-tTA;Teto-MYC, EμSR-tTA;Teto-MYC; E2f2*$^{-/-}$, *EμSR-tTA;Teto-MYC;p53*$^{-/-}$, *EμSR-tTA;Teto-MYC;Teto-Cre, Pten*$^{LoxP/LoxP}$, and *EμSR-tTA;Teto-MYC;Teto-Cre;Rosa26LOXP*^{EGFP} mice. *EμSR-tTA;Teto-MYC* mice were kept on a clean FVB/NJ genetic background. Tumor studies involving *p53*$^{-}$, *E2f2*$^{-}$ or *Pten*^{LoxP} alleles were performed with mice backcrossed into FVB/NJ mouse strain for five times (fifth generation). Mice of appropriate genotypes were monitored and harvested at the terminal stage as judged by the overall health of mice. Normal thymi or thymic tumor masses were homogenized to obtain single-cell suspensions from which red cells were removed using hypotonic cell lysis buffer (BD Pharmingen). Aliquots of cells were snap frozen in liquid nitrogen and used for DNA and RNA isolation as described below.

DNA isolation. Genomic DNA was isolated as described previously [45]. Briefly, 20–25 ml of preheated lysis buffer (150 mM EDTA pH 8.0, 10mM Tris HCl pH 8.0, and 1% Sarkosyl) was used to dissolve the tissue at 55 °C until the solution became homogenous. An equal amount of phenol:chloroform:isoamylalcohol (50:24:1) was used to extract the genomic DNA. Dialysis of the DNA solution was performed in 10 mM Tris HCL pH8.0 buffer overnight, and RNA was subsequently removed by digestion with RNaseA (500 μg/ml). Genomic DNA was precipitated with ethanol, dissolved in TE buffer, and stored at 4 °C.

RLGS. RLGS was performed according to the published protocol [46]. Briefly, 7 μg of DNA sample was used in each reaction. The ends of the sheared DNA were blocked with the addition of nucleotide analogs (αS-dGTP, αS-dCTP, ddATP, and ddTTP) using T4 DNA polymerase. DNA was then digested with 20 U of NotI enzyme (Promega) and generated sticky ends were filled in with [α-^{32}P]dCTP and [α-^{32}P]dGTP. The labeled DNA was then digested with 20 U Eco*R*V (Promega) and 0.7 μg was run on 0.8% agarose tube gel (first dimension separation) at 230 V for about 20 h. After electrophoresis, the DNA in the agarose gel was digested with 750 U of HinfI restriction enzyme (Promega) and then electrophoresed into 5% polyacrylamide gel (second dimension separation) at 150–180 V for 18–20 h. The gel was dried and autoradiography was performed on an X-ray film in the presence of one Quanta III intensifying screen (DuPont) at −80 °C for 3–21 d.

RLGS gel analysis. RLGS profiles obtained from tumors of different genotypes were compared to the profiles obtained from thymocytes of age-matched normal mice. RLGS fragments present in the profiles of normal thymocytes and absent or reduced in intensity in tumor profiles as determined by visual inspection relative to several neighboring unaltered NotI fragments were scored as DNA methylation events. Each RLGS profile was analyzed two times by independent investigators in a blinded fashion and loss events were scored only if the score was concordant between the two analyses. Loss events were scored as DNA methylation events regardless of the degree of intensity loss. RLGS fragments that were changed at least once within a genetic group from the initial analysis were subsequently marked for second round analysis to insure accuracy of obtained data. To avoid scoring polymorphic changes as DNA methylation events, all spots that showed variable intensity between RLGS profiles derived from FVB/NJ, 129SvIMJ, or C57BL/6J strains were removed [22].

Southern blotting. A total of 10 μg of genomic DNA isolated from normal thymocytes or thymic tumors was digested with NotI and EcoRV (New England Biolabs). Following electrophoretic separation using 0.8% agarose gels and transfer to GeneScreen nylon membranes (Perkin-Elmer), the digested DNA was probed with [α-^{32}P]dCTP radioactively labeled NotI-EcoRV DNA fragment as described before [47].

Bisulfite genomic sequencing and COBRA. One microgram of genomic DNA from tumors and normal controls was treated with sodium bisulfite according to published protocols [48]. Primers were designed to allow amplification of both methylated and unmethylated DNA. The sequences of primers used for each of the RLGS derived NotI-EcoRV fragments are listed in Table S3. For COBRA, the PCR product was digested using 10 U of restriction enzyme BstUI and separated on 8% polyacrylamide gel. For bisulfite sequencing, the PCR products were subcloned using the TOPO TA-Cloning kit (Invitrogen). Ten clones for each sample were sequenced using ABI big dye chemistry and compared to original genomic DNA sequence using Seqman 6.1 software (DNASTAR).

FACS. *EμSR-tTA;Teto-MYC;Teto-Cre;Rosa26LOXP*^{EGFP} mice were harvested at age 21, 31, or 42 d and thymocytes isolated from these mice were sorted for EGFP-positive and EGFP-negative cells using high-speed sorting with FACS Aria (Becton Dickinson). DNA and RNA was extracted from sorted cells and analyzed by RLGS and real-time RT-PCR. Lymphomas from terminally sick mice were characterized by using FACS. Briefly, single-cell suspensions prepared from thymic tumor masses were stained with antibodies specific for mouse T cells, B cells, myeloid and erythroid cells including anti-CD4, anti-CD8, anti-CD3, anti-B220, anti-CD11b, and anti-TER119 antibodies (BD Pharmingen). Stained cells were analyzed using FACSCalibur flow cytometer and CellQuest software (Becton Dickinson). All tumors analyzed in this study were T cell lymphomas and were negative for myeloid marker CD11b, B-cell marker B220, and erythroid marker TER119.

Quantitative real-time RT-PCR. Thymi or tumor masses were collected from mice of different ages and homogenized to obtain single cell suspensions that were used for total RNA isolation with TRIzol reagent according to manufacturer's instructions (Life Technologies). Two to 10 μg of total RNA were used to generate cDNA using Superscript III reverse transcriptase (Invitrogen). Real-time RT-PCR was performed using the BioRad iCycler PCR machine. Each PCR reaction contained 2.0 μl of cDNA template, primers at a concentration of 100 nM, and 1× SYBR Green Reaction Mix (BioRad). Reactions were performed in a final volume of 25 μl in triplicate and data were analyzed using the ΔCt method, where *GAPDH* served as the internal control. Each PCR generated only the expected amplicon, as shown by the melting-temperature profiles of the final products, gel electrophoresis, and sequencing. For Figure 4E, we chose threshold of 3-fold of reduction if range of fold repression for that gene in *EμSR-tTA;Teto-MYC*-derived tumors was less than 20-fold. If the gene was more severely repressed in *EμSR-tTA;Teto-MYC*-derived tumors (range exceeded 20-fold), we chose threshold of 5-fold

repression. Primer sequences used for expression studies are listed in Table S2.

Cell culture and retroviral infections. MEFs were isolated from E13.5 embryos using standard methods. All cells were cultured in DMEM with 15% fetal bovine serum. High titer retroviruses were produced by transient transfection of *pBABE-puro-MYC*, *pBABE-hygro Ras^{61L}* or *pBABE vector* plasmids into the Phoenix-Eco packaging cell line using standard methods. MEFs were infected three times at 12-h intervals with Phoenix cell supernatants containing 4 μg/ml of Sequabrene (Sigma). Infected cells were then selected for a total of 5 d in the presence of 2.5 μg/ml of puromycin and 200 μg/ml of hygromycin. At this point, cells infected with *MYC/Ras^{61L}* retroviruses showed transformed phenotype while cells infected with control virus retained normal phenotype. A portion of these cells was harvested and used for DNA isolation (C1 culture and C0 culture, respectively; Figure 3A). The rest of the *MYC*- and *Ras^{61L}*-transformed primary MEFs was kept either in culture or resuspended in serum-free DMEM medium at a concentration 1×10^7 cells/ml. Cells (100 ul) were injected subcutaneously into the right and left shoulders and hips of each 8–10-wk-old male athymic nude mouse. Tumors that developed in these mice were harvested 18 d after injection along with *MYC*- and *Ras^{61L}*-transformed primary MEFs kept in culture (tumors T2 and culture C2, respectively; Figure 3A). Cells and tumors developed in nude mice were used for DNA isolation and RLGS analysis.

Statistical analysis. DNA methylation frequencies in tumors derived from *EμSR-tTA;Teto-MYC, EμSR-tTA;Teto-MYC;E2f2$^{-/-}$*, *EμSR-tTA;Teto-MYC;p53$^{-/-}$*, and *EμSR-tTA;Teto-MYC;Teto-Cre;Pten$^{LoxP/LoxP}$* mice were compared across using nonparametric Kruskal-Wallis rank sum test [49]. Pair-wise comparisons of tumors deleted for either *p53*, *E2f2*, or *Pten* with those derived from *EμSR-tTA;Teto-MYC* mice were done by applying nonparametric Wilcoxon procedure [49] and were corrected for multiple comparisons with Bonferroni correction. A p-value < 0.0167 (0.05/3) was considered to be significant. Survival time data was analyzed the same way as above since there were no censored observations. Under the assumption that all samples within each group have the same frequency of methylation, the heterogeneity of DNA methylation frequencies across samples within each tumor group was assessed by comparing mean methylation frequencies to its variance using a chi-square statistic. Preferential methylation of RLGS fragments within each group was assessed under the null hypothesis of equal methylation frequencies for each fragment, using a goodness-of-fit test based on 10,000 random simulations. Hierarchical cluster analysis of samples was performed by applying phi-correlation coefficient [50] similarity metric with average linkage method, using all RLGS data with at least one methylation event across the respective samples. For each RLGS fragment, proportion of methylation between tumors from *EμSR-tTA;Teto-MYC* group and tumors derived from *EμSR-tTA;Teto-MYC;E2f2$^{-/-}$*, *EμSR-tTA;Teto-MYC;p53$^{-/-}$*, or *EμSR-tTA;Teto-MYC;Teto-Cre;Pten$^{LoxP/LoxP}$* groups, respectively, was compared by applying Fisher's exact test [49]. In order to identify RLGS fragments that showed an increase in methylation events compared to overall average methylation in the *EμSR-tTA;Teto-MYC* RLGS profiles, exact Binomial test [49] was applied.

Supporting Information

Figure S1. Methylation and Expression of RLGS Sequences
Found at doi:10.1371/journal.pgen.0030167.sg001 (3.2 MB PPT).

Figure S2. Bisulfite Sequencing of Selected RLGS Fragments
Found at doi:10.1371/journal.pgen.0030167.sg002 (852 KB PPT).

Figure S3. Absence of DNA Methylation in Precancerous Thymocytes
Found at doi:10.1371/journal.pgen.0030167.sg003 (3.1 MB PPT).

Figure S4. Overexpression of *MYC* in Precancerous Thymocytes Does Not Lead to Repression of Genes Methylated in Lymphomas
Found at doi:10.1371/journal.pgen.0030167.sg004 (485 KB PPT).

Figure S5. COBRA Analysis of Selected RLGS Fragments in Tumors Derived on Different Genotypes
Found at doi:10.1371/journal.pgen.0030167.sg005 (3.4 MB PPT).

Figure S6. Specific DNA Methylation Patterns in Genetic Subgroups
Found at doi:10.1371/journal.pgen.0030167.sg006 (55 KB PPT).

Table S1. Characterization of CpG Islands Methylated in Lymphomas
Found at doi:10.1371/journal.pgen.0030167.st001 (127 KB PPT).

Table S2. Primer Sequences for Real-Time RT-PCR
Found at doi:10.1371/journal.pgen.0030167.sg002 (47 KB PPT).

Table S3. Primer Sequences for COBRA Assays
Found at doi:10.1371/journal.pgen.0030167.sg003 (71 KB PPT).

Table S4. Random Forrest Analysis
Found at doi:10.1371/journal.pgen.0030167.sg004 (73 KB XLS).

Acknowledgments

RO and AR are supported by a T32 CA106196 fellowship in Cancer Genetics. SHW is supported by a fellowship from Susan G. Komen Breast Cancer Foundation. GL is the recipient of The Pew Charitable Trusts Scholar Award and the Leukemia & Lymphoma Society Scholar Award. CP is the recipient the Leukemia & Lymphoma Society Scholar Award.

Author contributions. RO, SHW, GL, and CP conceived and designed the experiments. RO, SHW, PT, AR, YH, YZW, BR, GL, and CP performed the experiments. RO, SHW, PT, AR, BK, SL RVD, GL, and CP analyzed the data. GW, MW, DF, MO, and CP contributed reagents/materials/analysis tools. RO, GL, and CP wrote the paper.

Funding. This work was funded by National Institutes of Health grants CA93548 and CA101956 (CP), P30 CA16058 (GL, CP), HD047470, and CA85619 (GL), and a translational award by the Leukemia & Lymphoma Society of America.

Competing interests. The authors have declared that no competing interests exist.

References

1. Jones PA, Baylin SB (2007) The Epigenomics of Cancer. Cell 128: 683–692.
2. Ehrlich M (2006) Cancer-linked DNA hypomethylation and its relationship to hypermethylation. Curr Top Microbiol Immunol 310: 251–274.
3. Jones PA, Baylin SB (2002) The fundamental role of epigenetic events in cancer. Nat Rev Genet 3: 415–428.
4. Esteller M, Corn PG, Baylin SB, Herman JG (2001) A gene hypermethylation profile of human cancer. Cancer Res 61: 3225–3229.
5. Feinberg AP, Tycko B (2004) The history of cancer epigenetics. Nat Rev Cancer 4: 143–153.
6. Yamada Y, Jackson-Grusby L, Linhart H, Meissner A, Eden A, et al. (2005) Opposing effects of DNA hypomethylation on intestinal and liver carcinogenesis. Proc Natl Acad Sci U S A 102: 13580–13585.
7. Costello JF, Plass C (2001) Methylation matters. J Med Genet 38: 285–303.
8. Feltus FA, Lee EK, Costello JF, Plass C, Vertino PM (2003) Predicting aberrant CpG island methylation. Proc Natl Acad Sci U S A 100: 12253–12258.
9. Bock C, Paulsen M, Tierling S, Mikeska T, Lengauer T, et al. (2006) CpG island methylation in human lymphocytes is highly correlated with DNA sequence, repeats, and predicted DNA structure. PLoS Genet 2: e26. doi:10.1371/journal.pgen.0020026
10. Das R, Dimitrova N, Xuan Z, Rollins RA, Haghighi F, et al. (2006) Computational prediction of methylation status in human genomic sequences. Proc Natl Acad Sci U S A 103: 10713–10716.
11. Brenner C, Deplus R, Didelot C, Loriot A, Vire E, et al. (2005) Myc represses transcription through recruitment of DNA methyltransferase corepressor. EMBO J 24: 336–346.
12. Di Croce L, Raker VA, Corsaro M, Fazi F, Fanelli M, et al. (2002) Methyltransferase recruitment and DNA hypermethylation of target promoters by an oncogenic transcription factor. Science 295: 1079–1082.
13. Liu S, Shen T, Huynh L, Klisovic MI, Rush LJ, et al. (2005) Interplay of RUNX1/MTG8 and DNA methyltransferase 1 in acute myeloid leukemia. Cancer Res 65: 1277–1284.
14. Bestor TH (2003) Unanswered questions about the role of promoter methylation in carcinogenesis. Ann N Y Acad Sci 983: 22–27.
15. Costello JF, Fruhwald MC, Smiraglia DJ, Rush LJ, Robertson GP, et al. (2000) Aberrant CpG-island methylation has non-random and tumour-type-specific patterns. Nat Genet 24: 132–138.
16. Issa JP (2004) CpG island methylator phenotype in cancer. Nat Rev Cancer 4: 988–993.
17. Yamashita K, Dai T, Dai Y, Yamamoto F, Perucho M (2003) Genetics supersedes epigenetics in colon cancer phenotype. Cancer Cell 4: 121–131.
18. Ogino S, Cantor M, Kawasaki T, Brahmandam M, Kirkner GJ, et al. (2006) CpG island methylator phenotype (CIMP) of colorectal cancer is best characterised by quantitative DNA methylation analysis and prospective cohort studies. Gut 55: 1000–1006.
19. Weisenberger DJ, Siegmund KD, Campan M, Young J, Long TI, et al. (2006) CpG island methylator phenotype underlies sporadic microsatellite

instability and is tightly associated with BRAF mutation in colorectal cancer. Nat Genet 38: 787–793.
20. Toyota M, Ohe-Toyota M, Ahuja N, Issa JP (2000) Distinct genetic profiles in colorectal tumors with or without the CpG island methylator phenotype. Proc Natl Acad Sci U S A 97: 710–715.
21. Yu L, Liu C, Bennett K, Wu YZ, Dai Z, et al. (2004) A NotI-EcoRV promoter library for studies of genetic and epigenetic alterations in mouse models of human malignancies. Genomics 84: 647–660.
22. Yu L, Liu C, Vandeusen J, Becknell B, Dai Z, et al. (2005) Global assessment of promoter methylation in a mouse model of cancer identifies ID4 as a putative tumor-suppressor gene in human leukemia. Nat Genet 37: 265–274.
23. Felsher DW, Bishop JM (1999) Reversible tumorigenesis by MYC in hematopoietic lineages. Mol Cell 4: 199–207.
24. Akama TO, Okazaki Y, Ito M, Okuizumi H, Konno H, et al. (1997) Restriction landmark genomic scanning (RLGS-M)-based genome-wide scanning of mouse liver tumors for alterations in DNA methylation status. Cancer Res 57: 3294–3299.
25. Rush LJ, Dai Z, Smiraglia DJ, Gao X, Wright FA, et al. (2001) Novel methylation targets in de novo acute myeloid leukemia with prevalence of chromosome 11 loci. Blood 97: 3226–3233.
26. Rush LJ, Raval A, Funchain P, Johnson AJ, Smith L, et al. (2004) Epigenetic profiling in chronic lymphocytic leukemia reveals novel methylation targets. Cancer Res 64: 2424–2433.
27. Dai Z, Lakshmanan RR, Zhu WG, Smiraglia DJ, Rush LJ, et al. (2001) Global methylation profiling of lung cancer identifies novel methylated genes. Neoplasia 3: 314–323.
28. Passegue E, Wagers AJ, Giuriato S, Anderson WC, Weissman IL (2005) Global analysis of proliferation and cell cycle gene expression in the regulation of hematopoietic stem and progenitor cell fates. J Exp Med 202: 1599–1611.
29. Vazquez F, Devreotes P (2006) Regulation of PTEN function as a PIP3 gatekeeper through membrane interaction. Cell Cycle 5: 1523–1527.
30. Pietsch EC, Humbey O, Murphy ME (2006) Polymorphisms in the p53 pathway. Oncogene 25: 1602–1611.
31. Suzuki A, Yamaguchi MT, Ohteki T, Sasaki T, Kaisho T, et al. (2001) T cell-specific loss of Pten leads to defects in central and peripheral tolerance. Immunity 14: 523–534.
32. Blyth K, Terry A, O'Hara M, Baxter EW, Campbell M, et al. (1995) Synergy between a human c-myc transgene and p53 null genotype in murine thymic lymphomas: contrasting effects of homozygous and heterozygous p53 loss. Oncogene 10: 1717–1723.
33. Cully M, You H, Levine AJ, Mak TW (2006) Beyond PTEN mutations: the PI3K pathway as an integrator of multiple inputs during tumorigenesis. Nat Rev Cancer 6: 184–192.
34. Hemann HT, Bric A, Teruya-Feldstein J, Herb A, Nilsson JA, et al. (2005) Nature 436,: 807–811
35. Nakamura M, Kishi M, Sakaki T, Hashimoto H, Nakase H, et al. (2003) Novel tumor suppressor loci on 6q22–23 in primary central nervous system lymphomas. Cancer Res 63: 737–741.
36. Kane MF, Loda M, Gaida GM, Lipman J, Mishra R, et al. (1997) Methylation of the hMLH1 promoter correlates with lack of expression of hMLH1 in sporadic colon tumors and mismatch repair-defective human tumor cell lines. Cancer Res 57: 808–811.
37. Herman JG, Umar A, Polyak K, Graff JR, Ahuja N, et al. (1998) Incidence and functional consequences of hMLH1 promoter hypermethylation in colorectal carcinoma. Proc Natl Acad Sci U S A 95: 6870–6875.
38. Agrelo R, Cheng WH, Setien F, Ropero S, Espada J, et al. (2006) Epigenetic inactivation of the premature aging Werner syndrome gene in human cancer. Proc Natl Acad Sci U S A 103: 8822–8827.
39. Feldman N, Gerson A, Fang J, Li E, Zhang Y, et al. (2006) G9a-mediated irreversible epigenetic inactivation of Oct-3/4 during early embryogenesis. Nat Cell Biol 8: 188–194.
40. Tagoh H, Ingram R, Wilson N, Salvagiotto G, Warren AJ, et al. (2006) The mechanism of repression of the myeloid-specific c-fms gene by Pax5 during B lineage restriction. EMBO J 25: 1070–1080.
41. Stirzaker C, Song JZ, Davidson B, Clark SJ (2004) Transcriptional gene silencing promotes DNA hypermethylation through a sequential change in chromatin modifications in cancer cells. Cancer Res 64: 3871–3877.
42. Hedenfalk I, Duggan D, Chen Y, Radmacher M, Bittner M, et al. (2001) Gene-expression profiles in hereditary breast cancer. N Engl J Med 344: 539–548.
43. van 't Veer LJ, Dai H, van de Vijver MJ, He YD, Hart AA, et al. (2002) Gene expression profiling predicts clinical outcome of breast cancer. Nature 415: 530–536.
44. Esteller M, Fraga MF, Guo M, Garcia-Foncillas J, Hedenfalk I, et al. (2001) DNA methylation patterns in hereditary human cancers mimic sporadic tumorigenesis Hum. Mol. Genet 10,: 3001–3007
45. Okazaki Y, Okuizumi H, Sasaki N, Ohsumi T, Kuromitsu J, et al. (1995) An expanded system of restriction landmark genomic scanning (RLGS Ver. 1.8). Electrophoresis 16: 197–202.
46. Costello JF, Plass C, Cavenee WK (2002) Restriction landmark genome scanning. Methods Mol Biol 200: 53–70.
47. Wu L, de Bruin A, Saavedra HI, Starovic M, Trimboli A, et al. (2003) Extra-embryonic function of Rb is essential for embryonic development and viability. Nature 421: 942–947.
48. Liu TH, Raval A, Chen SS, Matkovic JJ, Byrd JC, et al. (2006) CpG island methylation and expression of the secreted frizzled-related protein gene family in chronic lymphocytic leukemia. Cancer Res 66: 653–658.
49. Hollander M, Wolfe D (1999) Nonparametric statistical methods, 2nd Edition. New York: John Wiley & Sons Inc.
50. Cohen J, Cohen P (1983) Applied multiple regression/correlation analysis for the behavioral sciences, 2nd Edition. Hillsdale (New Jersey): Lawrence Erlbum Associates.